Published in final edited form as:
J Immunol. 2012 April 1; 188(7): 3332–3341. doi:10.4049/jimmunol.1102322.

Intrinsic differences in the initiation of B cell receptor signaling favor responses of human IgG$^+$ memory B cells over IgM$^+$ naïve B cells

Angel M. Davey and **Susan K. Pierce**[*]
Laboratory of Immunogenetics, National Institute of Allergy and Infectious Diseases, National Institutes of Health, Rockville, Maryland 20852

Abstract

The acquisition of long-lived memory B cells (MBCs) is critical for the defense against many infectious diseases. Despite their importance, little is known about how antigens (Ags) trigger human MBCs, even though our understanding of the molecular basis of Ag activation of B cells in model systems has advanced considerably. Here, we use quantitative, high-resolution, live cell imaging at the single cell and single molecule levels to describe the earliest Ag-driven events in human isotype-switched, IgG-expressing MBCs and compare them to those in IgM-expressing naïve B cells. We show that human MBCs are more robust than naïve B cells at each step in the initiation of B cell receptor (BCR) signaling, including interrogation of Ag-containing membranes, formation of sub-microscopic BCR oligomers and recruitment and activation of signaling-associated kinases. Despite their robust response to Ag, MBCs remain highly sensitive to FcγRIIB-mediated inhibition. We also demonstrate that in the absence of Ag, a portion of MBC receptors spontaneously oligomerized and phosphorylated kinases accumulated at the membrane and speculate that heightened constitutive signaling may play a role in maintaining MBC longevity. Using high-resolution imaging we have provided a description of the earliest events in the Ag activation of MBCs and evidence for acquired cell-intrinsic differences in the initiation of BCR signaling in human naïve and MBCs.

Introduction

The acquisition of antibody (Ab) memory is critical for protection from many human infectious diseases and is the basis for most current human vaccines (1, 2). Re-exposure to antigens (Ags) induces rapid, high-titered, high-affinity Ab responses that are mediated by an expanded memory B cell (MBC) population expressing somatically mutated, isotype-switched IgG B cell receptors (BCRs) (3). In contrast, primary Ab responses involve naïve B cells that express low affinity, unswitched IgM and IgD BCRs. It is likely that ability to develop vaccines for infectious diseases for which we have none, including malaria and AIDS, would benefit from a thorough understanding of the biology of memory B cells (MBCs).

A variety of studies comparing gene expression profiles, cellular phenotypes and responses to diverse stimuli have provided evidence of intrinsic differences in human naïve and MBCs that may allow MBCs to respond more efficiently than naïve B cells in secondary Ab responses (4). As compared to naïve B cells, MBCs were shown to have increased

[*]Address correspondence and reprint requests to: Dr. Susan K. Pierce, National Institute of Allergy and Infectious Diseases/National Institutes of, Health/Twinbrook II, 12441 Parklawn Drive, Room 200B, MSC 8180, Rockville, MD 20852 USA, Phone: (301) 496-9589, Fax: (301) 402-0259, spierce@nih.gov.

expression of genes involved in activation, costimulation and survival (5–7), to have a greater proliferative capacity and to produce more Ab-secreting plasma cells in response to a variety of stimuli including IL-2, IL-10, CD40L, Toll-like receptor ligands and anti-Ig (8–12). Taken together, these results define MBCs as long-lived, quiescent B cells that express high-affinity, somatically mutated, isotype-switched BCRs and are differentiated to respond rapidly to external stimuli, giving them an intrinsic advantage over naïve B cells in immune responses.

Although our understanding of the biology of MBCs has advanced recently, what remains largely unknown is the molecular basis of Ag activation of MBCs despite the fact that our understanding of BCR signaling in model systems has advanced considerably. B cell responses to Ags begin when Ags bind to the BCRs, resulting in BCR clustering and recruitment of the first kinases in the BCR signaling cascade, including Lyn and Syk that trigger at least four different signaling cascades (13–16). Our understanding of where B cells engage Ag and initiate signaling has also advanced (17). Although B cells can respond to Ag in solution, B cells were shown to respond robustly to Ag presented on Ag presenting cells (APCs) *in vitro* (18). Moreover, the use of two photon laser scanning microscopy has provided strong evidence that B cells recognize Ag on APCs *in vivo* (19–22). Through the application of live cell imaging techniques it has recently become possible to view the earliest events in Ag-driven B cell activation that trigger the downstream signaling cascades (23, 24). High-resolution imaging has provided a detailed picture of how B cells engage Ag presented on membrane surfaces and respond to it. Fleire *et al*. (25) first described the remarkably dynamic nature of B cell Ag engagement. They observed for mouse primary B cells that during the first two minutes after contact with Ag-containing bilayers, the BCRs form microclusters that trigger B cells to spread over the bilayer and to accumulate BCRs at the interface of the cell and the bilayer leading to B cell activation. We characterized the BCR-intrinsic events leading up to microcluster formation using single-molecule tracking, live cell imaging and provided evidence in mouse cells that Ag binding to BCRs leads to the formation of submicroscopic, immobile signaling active BCR oligomers by a novel mechanism that involves interactions between the BCR's mIg membrane-proximal ectodomains (26). Following oligomerization, BCR microclusters grew with time in both the number of BCRs in the cluster and the area of the cluster and the size of the cluster correlated with strength of signal (27). We demonstrated that IgG BCRs, as compared to IgM BCRs, more efficiently formed clusters that grew more rapidly and signaled more robustly (27). These studies established that intrinsic properties of IgG BCRs accounted for their enhanced ability to cluster and signal. Our understanding of the initiation of BCR signaling has come from the study of mouse model systems and to date these events have not been investigated in human B cells or in MBCs of either mice or humans.

Evidence is also accumulating that the early events in B cell activation are regulated by B cell coreceptors. We showed in mouse B cells that FcγRIIB, a potent inhibitory B cell coreceptor (28), when coligated to the BCR through immune complexes, blocked the earliest events in BCR signaling in primary mouse B cells, including BCR oligomerization, microcluster growth and cell spreading (29). Whether FcγRIIB regulation of BCR signaling is similar in naïve and MBCs in either mice or humans has not been investigated in detail. Diamond and colleagues reported that the expression of FcγRIIB was upregulated on human MBCs as compared to naïve human B cells (30), but failed to be upregulated on MBCs in patients with systemic lupus erythematosus (SLE). The failure to increase expression of FcγRIIB correlated with the decreased ability of FcγRIIB to regulate BCR signaling in SLE, suggesting a critical role for FcγRIIB in the regulation of human MBCs.

In this study, we use quantitative total internal reflection fluorescence (TIRF) microscopy at the single cell and single molecule levels to investigate the early Ag-driven events in IgM^+

and isotype-switched IgG^+ human peripheral blood (PB) B cells as representative of naïve and MBCs, respectively. We provide evidence that the quality of the earliest events in B cell activation distinguish naïve versus MBCs. We show that these early events are highly sensitive to inhibition by FcγRIIB. We also describe cell-intrinsic differences in constitutive BCR signaling in naïve and MBCs that could contribute to the longevity of MBCs.

Materials and Methods

Cells and Abs

B cells were purified from PBMCs from healthy, anonymous, adult blood bank donors via negative selection magnetic cell separation using a human B cell isolation kit II from Miltenyi (Germany). Human B cells were frozen in fetal bovine serum (FBS) (Gibco, Grand Island, NY) containing 7.5% dimethyl sulfoxide (DMSO; Sigma-Aldrich, St. Louis, MO), kept at −80°C for at least 24 hours, and then stored at −196°C in liquid nitrogen before use. B cells were thawed and washed in media (RPMI 1640 with L-Glutamine, Penicillin/Streptomycin 100 IU/ml, 10% heat-inactivated FBS, 50 μM β-Mercaptoethanol) immediately prior to each experiment as described by Crompton *et al*. (31).

Cy3 and DyLight 649-conjugated Fab goat Abs specific for human IgM, or $Fc_{5\mu}$-specific (Fab anti-IgM) were purchased from Jackson ImmunoResearch Laboratories (West Grove, PA). DyLight 649-Fab anti-IgG was either obtained from Jackson ImmunoResearch Laboratories or prepared by conjugating intact Fc_{γ}-specific Ab to DyLight 649 using an Ab labeling kit (Pierce, Rockford, IL) and subsequently preparing Fabs using a Fab micro preparation kit with Protein A/G purification (Pierce). A ‘nonblocking’ Fab mouse mAb specific for human FcγRIIB (clone no. 3H7) (Fab anti-FcγRIIB) was provided by Macrogenics (Rockville, MD) and conjugated to Alexa Fluor 568 using an Ab labeling kit (Molecular Probes, Eugene, OR). Cy3-labeled Fab mouse Ab pan specific for human major histocompatibility complex class I (Cy3-Fab anti-MHC-I) was prepared from intact Ab purchased from AbD Serotec (Raleigh, NC) by conjugating the Ab to Cy3 using an Ab labeling kit (Amersham, Piscataway, NJ) and preparing Fabs using a Fab micro preparation kit with Protein A purification (Pierce). Mouse mAb specific for human CD27 (anti-CD27) (EXBIO, Czech Republic) was conjugated to Alexa Fluor 568 using an Ab labeling kit (Molecular Probes) and Fabs were prepared using a Fab micro preparation kit with Protein A purification (Pierce). Rabbit Abs specific for phospho-ZAP70 (Ptyr319)-Syk (Tyr352) (anti-pSyk) and for phospho-PI3K p85 (Tyr458)/p55 (Tyr199) (anti-pPI3K) were from Cell Signaling (Danvers, MA). Rabbit Abs specific for phospho-ERK1 (Thr202/Tyr204)/ERK2 (Thr185/Tyr187) (anti-pERK), and for phospho-p38 MAPK (Thr180/Tyr182) (anti-pp38) were from R&D Systems. Primary Abs were detected using Alexa Fluor 488-conjugated $F(ab')_2$ goat Ab specific for rabbit IgG (H+L).

Biotin-conjugated $F(ab')_2$ goat Ab specific for human IgG + IgM (H+L) (biotin-$F(ab')_2$ anti-Ig) was purchased from Jackson ImmunoResearch Laboratories and used unlabeled, or was conjugated to Alexa Fluor 568 using an Ab labeling kit (Molecular Probes). $F(ab')_2$ goat Ab specific for human kappa light chain ($F(ab')_2$ anti-κ was purchased from MyBioSource (San Diego, CA), biotin-conjugated using EZ-Link Sulfo-NHS-LC-Biotin (Pierce) and used unlabeled, or conjugated to Alexa Fluor 568. Biotin-conjugated mouse mAb specific for human FcγRIIB (clone no. AT10) (biotin-anti-FcγRIIB) was purchased from AbD Serotec.

Preparation of anti-Ig-containing planar lipid bilayers

Planar fluid lipid bilayers were prepared as described previously (32–34) on Nanostrip (Cyantek, Freemont, CA) cleaned glass coverslips attached to the bottom of LabTek chambers (Thermo Fisher Scientific, Rochester, NY). As described by Sohn *et al*. (35),

biotin-containing lipid bilayers were prepared by fusing unilamellar vesicles of 99% 1,2-dioleoyl-sn-glycero-3-phosphocholine (DOPC) and 1% 1,2-dioleoyl-sn-glycero-3-phosphoethanolamine-cap-biotin (DOPE-cap-biotin) (Avanti Polar Lipids, Alabaster, AL) to the coverslips. Biotin-containing lipid bilayers were then incubated with 50 nM Streptavidin (Jackson Immunoresearch Laboratories) for 10 min, washed, and incubated with 10 nM biotin-F(ab′)$_2$ anti-Ig either alone, or in combination with 20 nM biotin-anti-FcγRIIB for 20 min.

Total internal reflection fluorescence (TIRF) microscopy and image analysis

TIRF images were acquired for live and fixed cells using an Olympus IX-81 microscope (Melville, NY) equipped with a TIRF port, CascadeII 512 × 512 electron-multiplying charge-coupled device (CCD) camera (Roper Scientific, Tucson, AZ), Olympus 100 × 1.45 N.A. objective lens, and heated stage maintained at 37°C. A 488-nm/514-nm argon gas laser and a 568-nm/647-nm red krypton/argon gas laser were employed as indicated. Alexa Fluor 488, Cy3, Alexa Fluor 568 and DyLight 649, were excited at 488-nm, 514-nm, 568-nm, and 647-nm and detected after 525/50 BP, 550/40 ET BP, 605/40 BP, and 665 LP emission filters, respectively, after a 488/568/647 or 514/647 dichroic filter wheel cube, as appropriate. Image acquisition was controlled by Metamorph software (Molecular Devices, Sunnyvale, CA), with a 100 ms exposure time for a 512 × 512 image, unless otherwise noted.

For live cell, time-lapse imaging, cells were incubated with 200 nM fluorescently labeled Fab anti-IgM and/or Fab anti-IgG, washed twice, and added to chambers containing planar lipid bilayers. When indicated, cells were also simultaneously incubated with 200 nM fluorescently labeled Fab anti-FcγRIIB or Fab anti-MHC-I or 200 nM Fab anti-CD27. To visualize the underlying anti-Ig (or anti-κ), 7% of the unlabeled biotin-F(ab′)$_2$ anti-Ig (or biotin-F(ab′)$_2$ anti-κ) was replaced with Alexa Fluor 568-labeled, biotin-F(ab′)$_2$ anti-Ig (or biotin-F(ab′)$_2$ anti-κ). TIRF images were acquired at 2 s intervals after loading the chamber with cells.

For fixed cell imaging, cells were prepared as described for live cell imaging and incubated on the bilayers for the indicated times. As described by Depoil *et al.* (36), the chambers were washed and the cells were fixed in 4% paraformaldehyde for 10 min at 37°C. Cells were permeabilized with 0.1% Triton X-100 for 5 min at 20°C and blocked with 1% BSA, 1% FCS, 1% goat serum and 0.05% Tween-20 in PBS. Cells were incubated with anti-pSyk, -pPI3K, -pERK, or -pp38 primary rabbit Abs and labeled with fluorescent F(ab′)$_2$ goat anti-rabbit IgG.

The contact area of B cells with anti-Ig containing lipid bilayers, the mean fluorescence intensity (mean FI) of BCR, anti-Ig, pSyk, pPI3K, pERK, or pp38 within the contact area (i.e., per unit area), and the number of pSyk microclusters per unit area were measured and counted using ImageJ software (National Institutes of Health, available at http://rsbweb.nih.gov/ij/). Unpaired two-tailed *t*-tests were performed for statistical comparisons (95% confidence interval). To monitor changes in the relative FI over the contact area during live cell, time-lapse imaging, the autotracking function of Image Pro Plus software (Media Cybernetics, Silver Spring, MD) was used (35). 3 × 3 pixel autotracking mode was used and the background FI outside the contact area was used as the lower-end threshold for segmentation. Individual BCR normalized FI curves were normalized to one before plotting with other curves on a single graph. For these time-lapse measurements, statistical significance (95% confidence interval) was assessed using the ‘compareGrowthCurves’ function from the statmod statistical modeling package (available at http://bioinf.wehi.edu.au/software/compareCurves) available from the R Project for Statistical Computing.

Linear regression analyses were conducted to assess the relationship between pSyk cluster number or mean FI and B cell contact area or BCR mean FI from fixed cell images using Prism software (GraphPad, LaJolla, CA). Colocalization between the BCR and the underlying anti-Ig or FcγRIIB was quantified from background subtracted images via intensity correlation analysis as described by Li *et al*. (37) using the WCIF plugin of ImageJ to obtain the Pearson's correlation index (29), and unpaired two-tailed *t*-tests were again performed for statistical comparisons.

Single particle tracking and analysis

For single molecule TIRF imaging, human B cells were labeled with 0.025 nM or 0.25 nM DyLight 649-Fab anti-IgM or anti-IgG, respectively, such that single BCR molecules could be visualized without the need for photobleaching (26). Cells were washed three times after labeling, incubated with Ag-presenting lipid bilayers for 5–10 min and imaged with a 633-nm laser at 5 mW (at the objective lens in epifluorescence mode). To achieve an exposure time of 35 ms, a 100 × 100 pixel region of interest was used for imaging, and streamline acquisition mode was used to image single BCR molecules for 300 frames over approximately 10 s. Data from at least 20 cells was acquired for each condition in each experiment.

The processing of single molecule TIRF videos was detailed previously (26), with tracking and analysis performed using Matlab (The Mathworks, Natick, MA) code based on available tracking algorithms (38, 39) (available at http://physics.georgetown.edu/). Trajectories were visually inspected and occasional tracking errors were corrected manually. A two dimensional-Gaussian fit was used to refine the positions of the diffraction-limited spots in the trajectories. Mean square displacement (MSD) and instant diffusion coefficients for each of a BCR molecule's trajectories were calculated from positional coordinates as described by Douglass and Vale (38, 39). Short-range single molecule diffusion coefficients ($\mu m^2/s$) were calculated from linear fits to MSD data of individual molecules for the time intervals 35–140 ms and plotted as cumulative probability distribution graphs. The proportion of diffusion slower than 0.01 $\mu m^2/s$ is classified as immobile (26), so the greater the immobile fraction, the slower the rate of diffusion.

Results

Early events in the response to membrane-bound anti-Ig distinguish human naïve B cells and MBCs

We used live cell TIRF microscopy to examine the early events that follow the encounter of IgM^+ and IgG^+ human PB B cells with anti-Ig, as a surrogate Ag, incorporated into lipid bilayers. We studied the B cell response to anti-Ig incorporated into lipid bilayers as a variety of studies have provided evidence that B cells are readily activated by Ag presented by APCs or incorporated into lipid bilayers as an APC mimic *in vitro* and using two-photon laser scanning fluorescence microscopy evidence was provided that recognition of Ag on APCs may be highly relevant to B cell activation *in vivo*. $CD19^+$ B cells were purified from PB mononuclear cells (PBMCs) by negative selection using Ab-coated magnetic beads and incubated with a mixture of Cy3-conjugated Fab goat Abs specific for human IgM (Cy3-Fab anti-IgM) and DyLight 649-conjugated Fab goat Abs specific for human IgG (DyLight 649-Fab anti-IgG) to label IgM^+ and IgG^+ B cells, respectively. The cells were washed and placed on fluid lipid bilayers that either contained or did not contain fluorescently labeled biotinylated $F(ab')_2$ goat Ab specific for human IgG + IgM (H+L) ($F(ab')_2$ anti-Ig) attached to streptavidin lipid incorporated into the bilayers. As measured by flow cytometry, ~1.3 fold more $F(ab')_2$ anti-Ig bound to IgG- versus IgM-expressing B cells (Figure S1A),

however IgG^+ B cells were slightly larger (~1.2 fold) than IgM^+ B cells (Figure S1B), indicating that the density of BCRs was similar on the two cell types.

Time lapse images showed that when IgM^+ or IgG^+ B cells were placed on bilayers that did not contain anti-Ig, the BCRs formed initial contact points with the bilayer, but did not spread substantially and did not cluster (Figure 1A, Video 1). When placed on anti-Ig-containing bilayers the BCRs of both IgM^+ and IgG^+ cells clustered upon contact with bilayers and the cells then rapidly spread over the bilayer (Figure 1A, Video 1). After maximal spreading, the cells showed a subtle contraction, with only a small inward movement of BCRs from the cell periphery. However, in contrast to the observations in mouse B cells (18, 25, 34) neither IgM^+ nor IgG^+ B cells formed well-organized immune synapses even after 10 min on the bilayers (not shown). We also imaged the fluorescently labeled anti-Ig in the bilayer (Figure 1A). Before B cells contacted the bilayer, the anti-Ig appeared evenly distributed, producing dim, uniform fluorescence intensity (FI). Upon B cell encounter, the anti-Ig accumulated underneath the B cell contact areas, resulting in what appears to be corresponding areas of anti-Ig FI that overlap with the areas of BCR FI to varying degrees.

To quantify the accumulation of BCRs at the interface of the B cell with the bilayer, we tracked several individual cells for three minutes, measuring the BCR FI within the contact area of B cells with the bilayers (Figure 1B). When placed on anti-Ig-containing bilayers, IgG^+ B cells accumulated BCRs in the contact area more rapidly than IgM^+ B cells, resulting in approximately 2 fold more BCRs after three min on the bilayer. The accumulation of the BCRs in the contact area was highly anti-Ig-dependent as neither IgG^+ nor IgM^+ B cells accumulated BCRs in the contact area in the absence of anti-Ig (Figure 1B). To ensure that the IgG and IgM BCRs did not behave differently due to differences in binding to anti-Ig, we also quantified BCR accumulation upon stimulation with biotinylated $F(ab')_2$ goat Abs specific for human κ light chain (anti-κ) incorporated into bilayers (Figure 1C). Although the overall levels of BCR accumulation were slightly lower with anti-κ stimulation as compared to anti-Ig stimulation, the differences in the rate and level of accumulation between IgG^+ and IgM^+ B cells were similar, confirming the generality of the observation made with anti-Ig. BCR accumulation was also quantified per unit area from images of IgM^+ and IgG^+ human B cells labeled as described for Figure 1A and fixed after 10 min of anti-Ig stimulation (Figure 1D). After 10 min on anti-Ig-containing bilayers the IgG^+ B cells accumulated more BCR mean FI per unit area at the interface of the B cell with the bilayer than did IgM^+ B cells.

The accumulation of BCR was selective for both IgM^+ and IgG^+ B cells as we observed no increase in MHC-I FI over the contact area in the absence of anti-Ig and only a slight, but not statistically significant, increase in the presence of anti-Ig (Figure 1E). Further, time-lapse TIRF images demonstrated that the MHC-I molecules did not co-localize with the BCR upon anti-Ig stimulation (Figure S2). This result indicates that MHC-I molecules neither accumulated in, nor were excluded from, the interface of the B cell with the bilayers.

We also imaged fluorescently labeled anti-Ig in the contact area of the B cell with the bilayer. For IgM^+ B cells, we observed that the anti-Ig FI increased at a rate similar to that of the BCR (Figure 1F), indicating that the BCRs that accumulated at the interface were bound to anti-Ig. In contrast, for IgG^+ B cells the BCR FI increased more rapidly than the anti-Ig FI between 30 s and 150 s after contact with the bilayer, indicating that a portion of IgG BCRs that were not bound by anti-Ig accumulated in the contact area in an anti-Ig-ligation-independent fashion. Consistent with this observation, although both IgM and IgG BCRs appeared to colocalize with anti-Ig to a relatively high degree (Figure 1A), when colocalization was quantified and given as a Pearson's correlation co-efficient it is clear that

fewer IgG BCRs colocalized with anti-Ig than did IgMBCRs (Figure S3). We observed a similar phenomenon when B cells were stimulated with anti- κ incorporated into the bilayer. For IgM^+ B cells the BCR and anti-κ FI increased at similar rates in the contact area (Figure 1G). However, for IgG^+ B cells a portion of BCRs accumulated in an anti-Ig-ligation-independent manner for the first 150 s on the bilayer. This Ag-ligation-independent accumulation of IgG BCRs may be a mechanism that allows MBCs to rapidly amplify BCR signaling at the initiation of the response.

BCRs on MBCs readily oligomerize in response to anti-Ig

Our previous studies in mouse B cells demonstrated that one of the earliest events following the B cell's encounter with membrane-associated Ag is the formation of signaling-active immobile BCR oligomers (26). To compare the formation of immobile BCR oligomers on human naïve versus MBCs, we used single molecule TIRF microscopy to monitor the diffusion of the BCRs on cells after placing them on bilayers that either contained anti-Ig or not. Time lapse imaging showed that the mobility of single BCR molecules was inhibited upon anti-Ig binding (Video 2). To quantify the extent of formation of immobile BCR oligomers, cumulative probability distributions were compiled from greater than 1000 single molecule trajectories (Figure 2A). For both IgM- and IgG-expressing B cells placed on bilayers that do not contain anti-Ig, a fraction of BCRs were immobile (diffusion coefficient ≤ 0.01 $\mu m^2/s$). This observation is consistent with previous studies of mouse primary B cells (26, 27, 40) and we have speculated that these spontaneous immobile BCR oligomers may play a role in tonic signaling (23). The IgG^+ cells showed a statistically significantly higher fraction of immobile oligomers as compared to IgM^+ cells (23% versus 17%) (Figure 2B) and the overall diffusion of the BCRs on IgG^+ cells was significantly slower as compared to IgM^+ cells (0.109 $\mu m^2/s$ versus 0.131 $\mu m^2/s$). When placed on anti-Ig-containing bilayers, the BCRs on IgG^+ cells more readily formed immobile BCR oligomers (46% immobile fraction and an average overall diffusion coefficient of 0.043 $\mu m^2/s$) as compared to those on IgM^+ cells (42% immobile fraction and an average overall diffusion coefficient of 0.062 $\mu m^2/s$) (Figure 2B), suggesting that MBCs are inherently better able to respond to the anti-Ig.

Enhanced anti-Ig-driven and constitutive kinase phosphorylation in MBCs as compared to naïve B cells

To determine if the differences observed between IgG^+ and IgM^+ human B cells in the early events of B cell activation resulted in enhanced signaling, we quantified the amount of pSyk, pPI3K, pERK and pp38 recruited to the B cell membrane by TIRF microscopy. B cells were labeled with Cy3-Fab anti-IgM and DyLight 649-Fab anti-IgG, placed on bilayers that either contained anti-Ig or did not for 10 min, fixed, permeabilized, stained with fluorescently labeled Abs specific for pSyk, pPI3K, pERK or pp38 and imaged. Levels of phosphorylated signaling molecules were quantified as either pSyk, pPI3K, pERK or pp38 FI over the B cell contact area or as the number of pSyk clusters. A representative image is given showing the BCR and pSyk distribution for IgM^+ and IgG^+ B cells (Figure 3A). The overall staining patterns for pPI3K, pERK and pp38 were similar to that of pSyk. The amount of pSyk recruited and the number of pSyk clusters was significantly higher for IgG^+ B cells as compared to IgM^+ cells ($p < 0.0001$ in both cases) (Figure 3A). In both cases the pSyk recruited to the membrane colocalized with the BCR. However, the pSyk to BCR FI ratios were similar for anti-Ig stimulated IgM^+ and IgG^+ B cells ($p = 0.072$), indicating that the individual IgG BCR microclusters were not more signaling-active than IgM BCR microclusters. Because the contact area of IgG^+ B cells with the anti-Ig-containing lipid bilayer is greater than the area of IgM^+ B cells, to confirm that the higher pSyk levels observed for IgG^+ B cells were not simply a function of B cell size, we carried out correlation analyses. The results showed a positive correlation between BCR FI and pSyk

cluster number for both IgM^+ and IgG^+ cells that was even more pronounced for IgG^+ cells (Figure S4A). In contrast, pSyk cluster number did not correlate with the size of the contact area for either B cell type (Figure S4B).

The amount of pPI3K (Figure 3B), pERK (Figure 3C) and pp38 (Figure 3D) recruited to the membranes of IgG^+ cells placed on anti-Ig-containing bilayers was also significantly greater than the amount recruited to membranes of anti-Ig stimulated IgM^+ cells ($p < 0.0001$ in all cases). As was the case for pSyk, the ratio of pPI3K, pERK and pp38 FIs to BCR FIs were similar for naïve and MBCs. If cells were stimulated on anti-Ig-containing bilayers for only 2 min prior to fixation, phosphorylated kinase levels followed the same trend as that observed after 10 min of stimulation (data not shown).

For B cells placed on bilayers that did not contain anti-Ig, we observed little difference in pSyk FIs or cluster numbers between IgM^+ and IgG^+ cells (Figure 3A). In contrast, the amounts of pPI3K, pERK and pp38 at the membrane in resting IgG^+ B cells were significantly greater than those in resting IgM^+ B cells ($p < 0.0001$ in all cases) (Figure 3B–D), translating to a highly significant increase in the ratio of phosphorylated kinase FIs to BCR FIs. Given that the amount of pSyk at the membrane was not increased in MBCs in the absence of anti-Ig, the increase in pPI3K, pERK and pp38 may be through a Syk-independent pathway, possibly through CD19. For PI3K we determined that the BCR and pPI3K were not highly colocalized (not shown), consistent with this possibility.

Naïve and MBCs are sensitive to FcγRIIB-mediated inhibition

FcγRIIB is a key negative regulator of BCR signaling (28) that we recently showed blocked the early events in mouse naïve B cell signaling (29). To determine if early events in the activation of human naïve and MBCs are similarly affected by coengagement of the BCR and FcγRIIB, B cells were labeled with DyLight 649-Fab anti-IgM or -IgG, and with a non-blocking Alexa Fluor 568-conjugated Fab mouse mAb specific for human FcγRIIB (Alexa 568-Fab anti-FcγRIIB). By flow cytometry IgG^+ cells expressed approximately 1.25 fold more FcγRIIB as compared to IgM^+ B cells (Figure S1C), as previously reported (30, 41) but because MBCs also express approximately 1.3 fold more BCRs, the ratio of FcγRIIB to BCRs is similar for the two cell types. The cells were washed and placed on bilayers containing biotinylated $F(ab')_2$ anti-Ig bound to streptavidin-lipid, either alone or in combination with biotinylated mouse mAb specific for human FcγRIIB (anti-FcγRIIB) to coligate the BCR and FcγRIIB. Timelapse images (Figure 4A) and the corresponding colocalization analysis at 60 s after stimulation (Figure 4B) showed that anti-Ig alone, in the absence of coligation to FcγRIIB, induced a significant increase in colocalization of the BCR and FcγRIIB in IgM^+ cells ($p = 0.012$) but not in IgG^+ cells ($p = 0.2$), suggesting that the FcγRIIB may play a role in BCR signaling in the absence of coligation in naïve B cells. Coligation of the BCR and FcγRIIB increased the colocalization of the BCR and FcγRIIB in both IgM^+ ($p = 0.0013$) and IgG^+ B cells ($p = 0.0011$) (Figure 4B) and reduced the accumulation of BCRs in the contact area with the anti-Ig-presenting membrane (Figure 4C) ($p < 0.0001$ in both cases).

The effect of BCR-FcγRIIB coligation on the accumulation of BCRs, anti-Ig and pSyk in the interface between the B cell and the bilayer was determined at later time points. IgM^+ and IgG^+ cells were placed on bilayers containing $F(ab')_2$ anti-Ig alone or in combination with anti-FcγRIIB for 2 or 10 min and then fixed. With BCR cross-linking alone, for both IgM^+ and IgG^+ B cells the amount of BCRs and anti-Ig that accumulated in the interface increased from 2 min (Figure 5A) to 10 min (Figure 5B) and BCR-FcγRIIB coligation blocked this accumulation, as well as the accumulation of pSyk.

CD27 expression correlates with enhanced efficiency of early BCR signaling events

Substantial heterogeneity among human MBCs has been documented by a variety of studies (4, 42, 43). At present, the relationship between the subsets and their relative contribution to long-lived B cell memory has not been established. For example, even though CD27 has been considered to be a marker for human MBCs, $CD27^-$ IgG^+ MBC populations have been reported (44) and conversely, a proportion of human $CD27^+$ B cells have not undergone isotype switching (45). We determined that approximately 70% of IgG^+ cells in PB were $CD27^+$, whereas only approximately 10% of IgM^+ cells were $CD27^+$ (data not shown). The B cells in the subpopulations defined by IgG, IgM and CD27 expression differed in size with: IgM^+ $CD27^-$ ≪ IgG^+ $CD27^-$ < IgM^+ $CD27^+$ = IgG^+ $CD27^+$ (Figure S1D). However, the origin and function of human IgM^+ $CD27^+$ MBCs remains controversial (4, 45). We investigated the early events in B cell activation and their sensitivity to FcγRIIB inhibition in IgM^+ and IgG^+ B cells that were either $CD27^-$ or $CD27^+$. B cells were labeled with either DyLight 649-Fab anti-IgM or -IgG and Alexa Fluor 568-conjugated Fab mouse Ab specific for human CD27 (Alexa 568-anti-CD27), placed on bilayers containing anti-Ig alone or in combination with anti-FcγRIIB for 10 min, fixed, permeabilized, stained with rabbit anti-pSyk detected using Alexa Fluor 488 $F(ab')_2$ secondary Ab to rabbit Ig and imaged. In the absence of anti-Ig stimulation, there were no significant differences in BCR accumulation or pSyk recruitment between IgG^+ $CD27^+$ and IgG^+ $CD27^-$ B cells or between IgM^+ $CD27^+$ and IgM^+ $CD27^-$ B cells, indicating that BCRs on $CD27^+$ B cells of either isotype are not in a more constitutively activated state as compared to those on $CD27^-$ B cells. Upon anti-Ig stimulation, as compared to IgM^+ $CD27^-$ B cells IgM^+ $CD27^+$ B cells accumulated more BCRs and pSyk ($p < 0.0001$ in both cases) in the interface between the B cell and the bilayer (Figure 6A). The anti-Ig-induced accumulation of BCRs and recruitment of pSyk were sensitive to FcγRIIB inhibition for both $CD27^+$ and $CD27^-$ IgM B cells. $CD27^+$ IgG^+ B cells also accumulated more BCRs and pSyk in the interface between the B cell and the bilayers as compared to IgG^+ B cells that did not express CD27 ($p < 0.0001$ in both cases) (Figure 6B). For both $CD27^+$ and $CD27^-$ IgG-expressing B cells, both BCR accumulation and pSyk recruitment were sensitive to FcγRIIB inhibition. However, a comparison of IgM^+ $CD27^+$ cells and IgG^+ $CD27^+$ cells showed that CD27 expression did not result in IgM^+ cells accumulating as much BCR and pSyk in the interface upon anti-Ig stimulation as IgG^+ cells ($p < 0.0001$ in both cases). Collectively, these results indicate that B cells that express CD27 are more responsive to anti-Ig than $CD27^-$ B cells. However, IgG BCRs are more efficient than IgM BCRs, independent of CD27 expression.

Discussion

Despite the key role that Ab memory plays in protection from a variety of infectious diseases (1, 2), little is known about the responses of human MBCs and naïve B cells to Ag. High-resolution live cell imaging is providing the tools necessary to define and order the early events in BCR signaling that ultimately lead to B cell proliferation and differentiation. Here, we used these tools to compare the responses of human PB IgM^+ B cells and IgG^+ B cells as representative naïve B cells and MBCs respectively. Our results show that human MBCs are more robust at each step in the initiation of BCR signaling, from interrogation of the lipid bilayer, to the formation of sub-microscopic BCR oligomers, to the recruitment and activation of kinases in the BCR signaling cascade. We recently provided evidence in mouse primary B cells that these early events in the initiation of BCR signaling were highly sensitive to the affinity of the BCR for Ag (40). As human MBCs have undergone somatic hypermutation and express high- affinity BCRs, we predict that in response to specific Ags, the differences in the response of human MBC and naïve B cells would be even more dramatic than that shown here using anti-Ig as a surrogate Ag. The robust responses of MBCs to anti-Ig and anti-κ that we observed *in vitro* could provide an advantage in

responding to Ag in the competitive environments of the lymphoid tissues *in vivo*, explaining in part the rapid, high-titered Ab responses characteristic of B cell memory. In addition, a number of studies have provided evidence for cell-intrinsic differences between human naïve and MBCs in gene expression and responses to a variety of stimuli, including T cell help, cytokines, TLR ligands and anti-Ig, that are consistent with the ability of MBCs to respond quickly and robustly during an immune response, giving MBCs an intrinsic advantage over naïve B cells (4). Such differences would serve to further amplify the intrinsic advantage conferred on MBCs through their efficient Ag-driven initiation of BCR signaling.

We observed in human B cells a new phenomenon that we first described in mouse IgG-expressing B cells (27), namely that IgG BCRs, unlike IgM BCRs, show an Ag-ligation-independent phase in the recruitment of BCRs to BCR-microclusters. From 30 s to 150 s following anti-Ig encounter, the FI of IgG BCRs in the interface between the B cells and the bilayer increased more quickly than did the FI of the underlying anti-Ig, indicating an accumulation of IgG BCRs that were not bound to anti-Ig. In contrast, the FIs of IgM BCRs and underlying anti-Ig accumulated at the same rate. We speculate that this may be a novel mechanism to rapidly amplify early IgG BCR signaling in MBCs.

We also found differences between naïve B cells and MBCs that were independent of BCR ligation. We observed that in the absence of anti-Ig, MBCs were more signaling active, having more spontaneously oligomerized BCRs that recruit more pPI3K, pERK and pp38 to the membranes. Rajewsky and colleagues recently demonstrated a key role of PI3K in BCR tonic signaling (46). These authors suggested that modulation of PI3K signaling may be the key element in the control of mature B cell survival mediated by the BCR. While studies have suggested that Ag binding is not required for the maintenance of IgG MBCs (47), the possibility that a constitutive or tonic BCR signal is needed has not been ruled out. In fact, Hikida *et al*. proposed that the BCR uses PLC-γ2 for MBC generation and maintenance (48), supporting the involvement of BCR signaling in maintaining MBC longevity. Other recent work suggested that tonic BCR signals are propagated via ERK showing that treatment with a MEK inhibitor blocked immature B cell differentiation and that immature B cells with low BCR expression were rescued by expression of a constitutively active N-Ras (49). It is possible that the higher constitutive level of pPI3K and pERK that we observed in MBCs plays a role in the survival of MBCs, allowing them to achieve their remarkable characteristic longevity. Adachi and Davis (50) recently provided evidence that the phosphorylation of ERK and p38 are dramatically different in naïve and Ag-experienced T cells following T cell receptor stimulation and suggested that these differences could account for differences in responses to Ag. It is possible that the difference in naïve and MBC recruitment of pERK and pp38 in resting cells may subsequently impact Ag-driven signaling in an analogous fashion.

We also show that the robust early responses of MBCs to anti-Ig were completely inhibited by coligating the BCR and FcγRIIB. Thus, differentiation to MBCs does not alter the B cell's sensitivity to FcγRIIB- mediated inhibition. We also observed a difference in the spatial relationship between the BCR and FcγRIIB following BCR crosslinking alone in naïve and MBCs. Only in naïve B cells did FcγRIIB show significant microscopic colocalization with the BCR. It is possible that the spatial proximity of FcγRIIB and the BCR serve to limit BCR signaling in naïve B cells.

It is becoming increasingly clear that MBCs are not a homogeneous subpopulation of cells, but rather a phenotypically and functionally heterogeneous population of Ag-experienced B cells (42, 43). CD27 expression was considered to be a reliable marker for human MBCs, but it has more recently become apparent that up to 30% of IgG^+ B cells are $CD27^-$. IgG^+

$CD27^+$ and IgG^+ $CD27^-$ subpopulations may have distinct origins and functions in memory responses. IgM^+ $CD27^+$ and IgM^+ IgD^+ $CD27^+$ human B cells have also been described, but their origins and functions remain less well understood. We found that B cells that expressed CD27 were more robust in the early events in B cell activation, but that IgG^+ $CD27^+$ B cells demonstrated stronger responses to anti-Ig than did IgM^+ $CD27^+$ cells.

Collectively our results suggest that differences in the early events following anti-Ig binding between IgM^+ naïve B cells and IgG^+ MBCs may explain in part the heightened recall Ab responses observed *in vivo*. A better understanding of the molecular mechanisms that determine the responses to Ag at the early stages of B cell activation in normal human naïve and MBCs may provide new strategies to attenuate this process in systemic autoimmune diseases and to design more effective vaccines.

Supplementary Material

Refer to Web version on PubMed Central for supplementary material.

Acknowledgments

We thank Dr. Wanli Liu for helpful suggestions and guidance and Dr. Joseph Brzostowski for expert advice on imaging in the NIH/NIAID-LIG Imaging Facility.

This work has been supported by the Intramural Research Program of the National Institutes of Health, National Institute of Allergy and Infectious Diseases.

Abbreviations used in this paper

ERK	extracellular signal-regulated protein kinase
FI	fluorescence intensity
MBC	memory B cell
p38	p38 MAP kinase
PB	peripheral blood
pERK	phosphorylated ERK
PI3K	phosphoinositide 3-kinase
pp38	phosphorylated p38
pPI3K	phosphorylated PI3K
pSyk	phosphorylated Syk
TIRF	total internal reflection fluorescence

References

1. Plotkin SA. Correlates of protection induced by vaccination. Clin Vaccine Immunol. 2010; 17:1055–1065. [PubMed: 20463105]
2. Sallusto F, Lanzavecchia A, Araki K, Ahmed R. From vaccines to memory and back. Immunity. 2010; 33:451–463. [PubMed: 21029957]
3. Wrammert J, Miller J, Akondy R, Ahmed R. Human immune memory to yellow fever and smallpox vaccination. J Clin Immunol. 2009; 29:151–157. [PubMed: 19052852]
4. Tangye SG, Tarlinton DM. Memory B cells: effectors of long-lived immune responses. Eur J Immunol. 2009; 39:2065–2075. [PubMed: 19637202]

5. Good KL, Avery DT, Tangye SG. Resting human memory B cells are intrinsically programmed for enhanced survival and responsiveness to diverse stimuli compared to naive B cells. J Immunol. 2009; 182:890–901. [PubMed: 19124732]
6. Klein U, Tu Y, Stolovitzky GA, Keller JL, Haddad J Jr, Miljkovic V, Cattoretti G, Califano A, Dalla-Favera R. Transcriptional analysis of the B cell germinal center reaction. Proc Natl Acad Sci U S A. 2003; 100:2639–2644. [PubMed: 12604779]
7. Good KL, Tangye SG. Decreased expression of Kruppel-like factors in memory B cells induces the rapid response typical of secondary antibody responses. Proc Natl Acad Sci U S A. 2007; 104:13420–13425. [PubMed: 17673551]
8. Arpin C, Banchereau J, Liu YJ. Memory B cells are biased towards terminal differentiation: a strategy that may prevent repertoire freezing. J Exp Med. 1997; 186:931–940. [PubMed: 9294147]
9. Tangye SG, Avery DT, Hodgkin PD. A division-linked mechanism for the rapid generation of Ig-secreting cells from human memory B cells. J Immunol. 2003; 170:261–269. [PubMed: 12496408]
10. Tangye SG, Avery DT, Deenick EK, Hodgkin PD. Intrinsic differences in the proliferation of naive and memory human B cells as a mechanism for enhanced secondary immune responses. J Immunol. 2003; 170:686–694. [PubMed: 12517929]
11. Bernasconi NL, Traggiai E, Lanzavecchia A. Maintenance of serological memory by polyclonal activation of human memory B cells. Science. 2002; 298:2199–2202. [PubMed: 12481138]
12. Bernasconi NL, Onai N, Lanzavecchia A. A role for Toll-like receptors in acquired immunity: up-regulation of TLR9 by BCR triggering in naive B cells and constitutive expression in memory B cells. Blood. 2003; 101:4500–4504. [PubMed: 12560217]
13. Campbell KS. Signal transduction from the B cell antigen-receptor. Curr Opin Immunol. 1999; 11:256–264. [PubMed: 10375554]
14. Kurosaki T. Genetic analysis of B cell antigen receptor signaling. Annu Rev Immunol. 1999; 17:555–592. [PubMed: 10358768]
15. DeFranco AL. The complexity of signaling pathways activated by the BCR. Curr Opin Immunol. 1997; 9:296–308. [PubMed: 9203421]
16. Dal Porto JM, Gauld SB, Merrell KT, Mills D, Pugh-Bernard AE, Cambier J. B cell antigen receptor signaling 101. Mol Immunol. 2004; 41:599–613. [PubMed: 15219998]
17. Batista FD, Harwood NE. The who, how and where of antigen presentation to B cells. Nat Rev Immunol. 2009; 9:15–27. [PubMed: 19079135]
18. Batista FD, Iber D, Neuberger MS. B cells acquire antigen from target cells after synapse formation. Nature. 2001; 411:489–494. [PubMed: 11373683]
19. Qi H, Egen JG, Huang AY, Germain RN. Extrafollicular activation of lymph node B cells by antigen-bearing dendritic cells. Science. 2006; 312:1672–1676. [PubMed: 16778060]
20. Carrasco YR, Batista FD. B cells acquire particulate antigen in a macrophage-rich area at the boundary between the follicle and the subcapsular sinus of the lymph node. Immunity. 2007; 27:160–171. [PubMed: 17658276]
21. Junt T, Moseman EA, Iannacone M, Massberg S, Lang PA, Boes M, Fink K, Henrickson SE, Shayakhmetov DM, Di Paolo NC, van Rooijen N, Mempel TR, Whelan SP, von Andrian UH. Subcapsular sinus macrophages in lymph nodes clear lymph-borne viruses and present them to antiviral B cells. Nature. 2007; 450:110–114. [PubMed: 17934446]
22. Phan TG, Grigorova I, Okada T, Cyster JG. Subcapsular encounter and complement-dependent transport of immune complexes by lymph node B cells. Nat Immunol. 2007; 8:992–1000. [PubMed: 17660822]
23. Pierce S, Liu W. The tipping points in the initiation of B cell signalling: how small changes make big differences. Nat Rev Immunol. 2010; 10:767–777. [PubMed: 20935671]
24. Harwood NE, Batista FD. New insights into the early molecular events underlying B cell activation. Immunity. 2008; 28:609–619. [PubMed: 18482567]
25. Fleire SJ, Goldman JP, Carrasco YR, Weber M, Bray D, Batista FD. B cell ligand discrimination through a spreading and contraction response. Science. 2006; 312:738–741. [PubMed: 16675699]
26. Tolar P, Hanna J, Krueger PD, Pierce SK. The constant region of the membrane immunoglobulin mediates B cell-receptor clustering and signaling in response to membrane antigens. Immunity. 2009; 30:44–55. [PubMed: 19135393]

27. Liu W, Meckel T, Tolar P, Sohn HW, Pierce SK. Intrinsic properties of immunoglobulin IgG1 isotype-switched B cell receptors promote microclustering and the initiation of signaling. Immunity. 2010; 32:778–789. [PubMed: 20620943]
28. Ravetch JV, Bolland S. IgG Fc receptors. Annu Rev Immunol. 2001; 19:275–290. [PubMed: 11244038]
29. Liu W, Won Sohn H, Tolar P, Meckel T, Pierce SK. Antigen-induced oligomerization of the B cell receptor is an early target of FcγRIIB inhibition. J Immunol. 2010; 184:1977–1989. [PubMed: 20083655]
30. Mackay M, Stanevsky A, Wang T, Aranow C, Li M, Koenig S, Ravetch JV, Diamond B. Selective dysregulation of the FcγIIB receptor on memory B cells in SLE. J Exp Med. 2006; 203:2157–2164. [PubMed: 16923849]
31. Crompton PD, Mircetic M, Weiss G, Baughman A, Huang CY, Topham DJ, Treanor JJ, Sanz I, Lee FE, Durbin AP, Miura K, Narum DL, Ellis RD, Malkin E, Mullen GE, Miller LH, Martin LB, Pierce SK. The TLR9 ligand CpG promotes the acquisition of Plasmodium falciparum-specific memory B cells in malaria-naive individuals. J Immunol. 2009; 182:3318–3326. [PubMed: 19234231]
32. Brian AA, McConnell HM. Allogeneic stimulation of cytotoxic T cells by supported planar membranes. Proc Natl Acad Sci USA. 1984; 81:6159–6163. [PubMed: 6333027]
33. Grakoui A, Bromley SK, Sumen C, Davis MM, Shaw AS, Allen PM, Dustin ML. The immunological synapse: a molecular machine controlling T cell activation. Science. 1999; 285:221–227. [PubMed: 10398592]
34. Carrasco YR, Fleire SJ, Cameron T, Dustin ML, Batista FD. LFA-1/ICAM-1 interaction lowers the threshold of B cell activation by facilitating B cell adhesion and synapse formation. Immunity. 2004; 20:589–599. [PubMed: 15142527]
35. Sohn HW, Tolar P, Pierce SK. Membrane heterogeneities in the formation of B cell receptor-Lyn kinase microclusters and the immune synapse. J Cell Biol. 2008; 182:367–379. [PubMed: 18644892]
36. Depoil D, Fleire S, Treanor BL, Weber M, Harwood NE, Marchbank KL, Tybulewicz VL, Batista FD. CD19 is essential for B cell activation by promoting B cell receptor-antigen microcluster formation in response to membrane-bound ligand. Nature immunology. 2008; 9:63–72. [PubMed: 18059271]
37. Li Q, Lau A, Morris TJ, Guo L, Fordyce CB, Stanley EF. A syntaxin 1, G alpha (o), and N-type calcium channel complex at a presynaptic nerve terminal: analysis by quantitative immunocolocalization. J Neurosci. 2004; 24:4070–4081. [PubMed: 15102922]
38. Douglass AD, Vale RD. Single-molecule microscopy reveals plasma membrane microdomains created by protein-protein networks that exclude or trap signaling molecules in T cells. Cell. 2005; 121:937–950. [PubMed: 15960980]
39. Douglass AD, Vale RD. Single-molecule imaging of fluorescent proteins. Method Cell Biol. 2008; 85:113–125.
40. Liu W, Meckel T, Tolar P, Sohn HW, Pierce SK. Antigen affinity discrimination is an intrinsic function of the B cell receptor. J Exp Med. 2010; 207:1095–1111. [PubMed: 20404102]
41. Su K, Yang H, Li X, Gibson AW, Cafardi JM, Zhou T, Edberg JC, Kimberly RP. Expression profile of FcγRIIb on leukocytes and its dysregulation in systemic lupus erythematosus. J Immunol. 2007; 178:3272–3280. [PubMed: 17312177]
42. Kurosaki T, Aiba Y, Komentani K, Moriyama S, Takahashi Y. Unique properties of memory B cells of different isotypes. Immunol Rev. 2010; 237:104–116. [PubMed: 20727032]
43. Sanz I, Wei C, Lee FE, Anolik J. Phenotypic and functional heterogeneity of human memory B cells. Semin Immunol. 2008; 20:67–82. [PubMed: 18258454]
44. Fecteau JF, Côté G, Néron S. A new memory $CD27^{-}IgG^{+}$ B cell population in peripheral blood expressing V_H genes with low frequency of somatic mutation. J Immunol. 2006; 177:3728–3726. [PubMed: 16951333]
45. Tangye SG, Good KL. Human $IgM^{+}CD27^{+}$ B cells: memory B cells or “memory” B cells? J Immunol. 2007; 179:13–19. [PubMed: 17579014]

46. Srinivasan L, Sasaki Y, Calado DP, Zhang B, Paik JH, DePinho RA, Kutok JL, Kearney JF, Otipoby KL, Rajewsky K. PI3 kinase signals BCR-dependent mature B cell survival. Cell. 2009; 139:573–586. [PubMed: 19879843]

47. Maruyama M, Lam KP, Rajewsky K. Memory B-cell persistence is independent of persisting immunizing antigen. Nature. 2000; 407:636–642. [PubMed: 11034213]

48. Hikida M, Casola S, Takahashi N, Kaji T, Takemori T, Rajewsky K, Kurosaki T. PLC-γ2 is essential for formation and maintenance of memory B cells. J Exp Med. 2009; 206:681–689. [PubMed: 19273623]

49. Rowland SL, DePersis CL, Torres RM, Pelanda R. Ras activation of Erk restores impaired tonic BCR signaling and rescues immature B cell differentiation. J Exp Med. 2010; 207:607–621. [PubMed: 20176802]

50. Adachi K, Davis MM. T-cell receptor ligation induces distinct signaling pathways in naïve vs. antigen-experienced T cells. Proc Natl Acad Sci U S A. 2010; 108:1549–1554. [PubMed: 21205892]

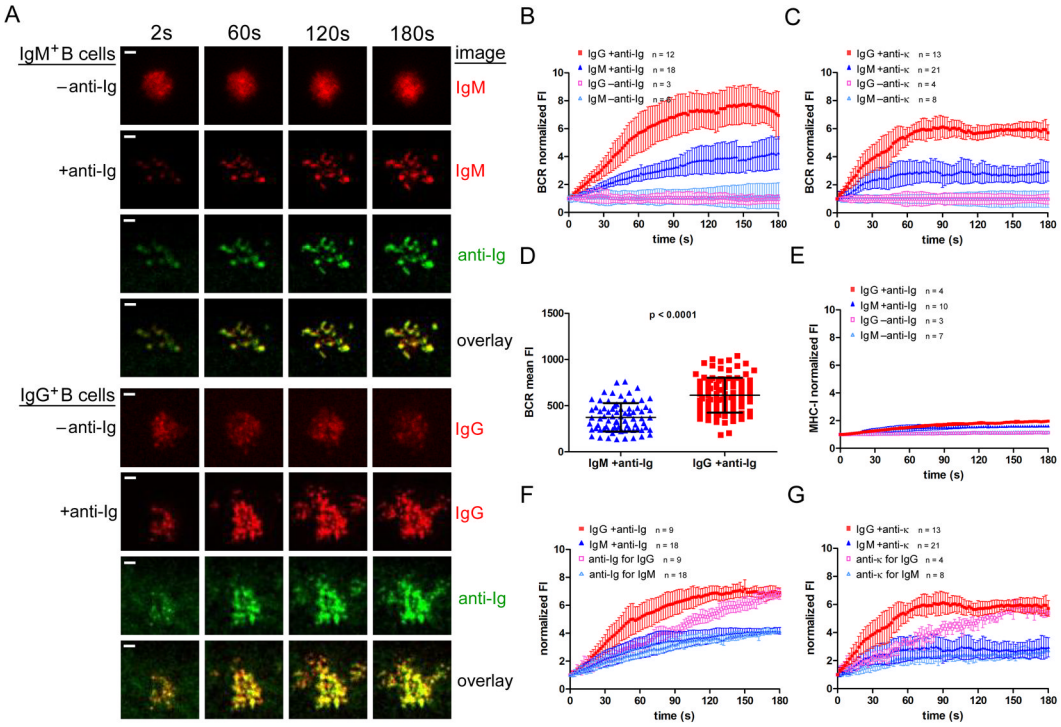

Figure 1. Interactions with anti-Ig- and anti-κ-containing lipid bilayers distinguish human MBCs and naïve B cells

(A) Representative time lapse TIRF images over 180 s (Video 1) of IgM^+ B cells (top panels) and IgG^+ B cells (bottom panels) placed on fluid lipid bilayers that did not contain $F(ab')_2$ anti-Ig (−anti-Ig) or did contain anti-Ig (+anti-Ig). The images shown are of: Cy3-Fab anti-IgM (top, red); DyLight 649-Fab anti-IgG (bottom, red); Alexa 568- $F(ab')_2$ anti-Ig (green) and the overlay of IgM and anti-Ig (top) or IgG and anti-Ig (bottom). (Scalebar = 1 μm.) Normalized BCR FI growth quantified from several timelapse image series over a period of 180 s for IgM^+ or IgG^+ B cells labeled as in (A) and placed on −anti-Ig or +anti-Ig fluid lipid bilayers (B) or on anti-κ^-or anti-κ^+ fluid lipid bilayers (C). (D) Statistical comparison of BCR mean FI accumulated within the B cell contact area per unit area as quantified from images of IgM^+ and IgG^+ human B cells labeled as in (A) and fixed after 10 min of anti-Ig stimulation. (E) Normalized MHC-I FI quantified from several time lapse image series over a period of 180 s for cells labeled cells with DyLight 649-Fab anti-IgM or -IgG and Cy3-Fab anti-MHC-I (Figure S2) and placed either on −anti-Ig or +anti-Igfluid lipid bilayers. Normalized BCR and anti-Ig FIs quantified from several image series over a period of 180 s for cells labeled with DyLight 649-Fab anti-IgM or anti-IgG and placed on (F) anti-Ig (Alexa 568- $F(ab')_2$ anti-Ig)-containing bilayers or on (G) anti-κ (Alexa 568- $F(ab')_2$ anti-κ)-containing bilayers. The data in (B), (D) and (F) and in (C), (E) and (G) were averaged over two and three independent experiments, respectively, and the bars indicate the mean ± SD.

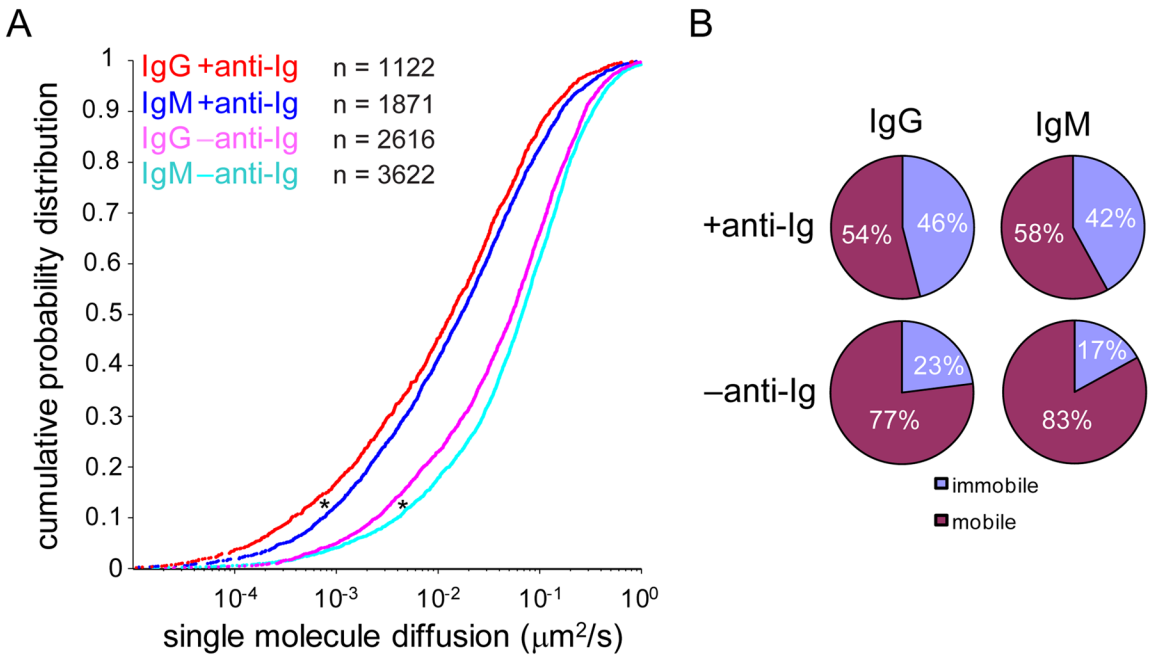

Figure 2. Immobile BCR oligomers form in response to anti-Ig-containing fluid lipid bilayers

(A) Cumulative probability plots of the diffusion coefficients of single BCR molecules were obtained from timelapse TIRF videos of IgM^+ (Video 2) and human B cells labeled with DyLight 649-Fab anti-IgM or -IgG and placed on −anti-Ig or +anti-Igbilayers. The numbers (n) of trajectories collected from two independent experiments and used to construct each probability curve are indicated on the graph. (*$p < 0.0001$.) (B) The percentages of BCR molecules in the mobile and immobile fractions, defined by a cutoff diffusion coefficient of 0.01 $\mu m^2/s$, are given.

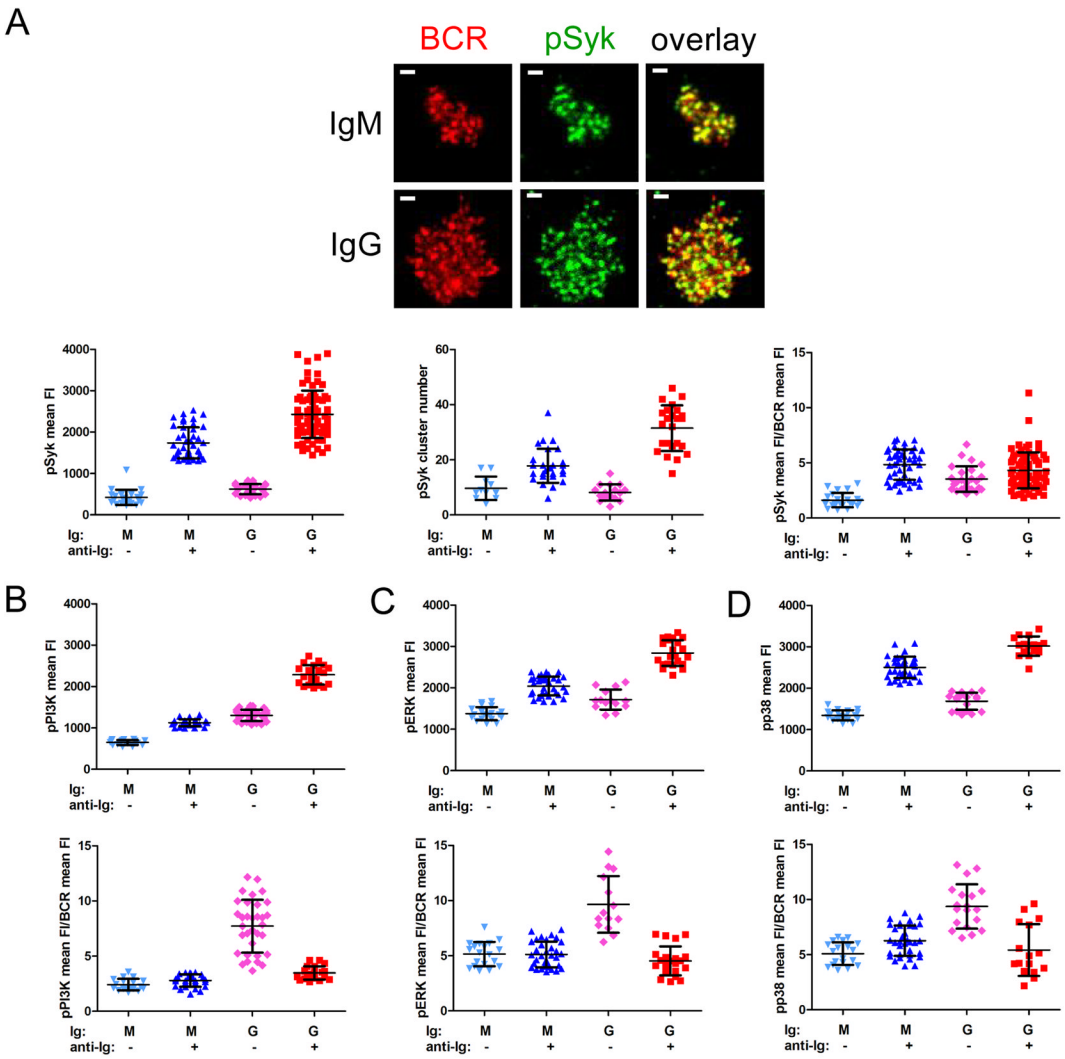

Figure 3. Phosphorylated kinases accumulate at the B cell membrane in response to anti-Ig-containing lipid bilayers

(A) Representative TIRF images show the BCR (red; labeled with DyLight 649-Fab anti-IgM or -IgG) and pSyk (green; rabbit anti-pSyk detected using Alexa 488-F(ab′)$_2$ rabbit Ig specific Abs) distribution for IgM$^+$ and IgG$^+$ human B cells placed on anti-Ig-containing fluid lipid bilayers for 10 min, fixed and labeled as described in the Materials and Methods. Also shown are the pSyk mean FI, pSyk cluster number and ratio of pSyk mean FI to BCR mean FI quantified from several TIRF images of B cells placed on +anti-Ig (or −anti-Ig) bilayers. Each data point represents one cell analyzed in one of three independent experiments and the bars indicate the mean ± SD. (B) The pPI3K mean FI and the ratio of pPI3K mean FI to BCR mean FI, (C) the pERK mean FI and the ratio of pERK mean FI to BCR mean FI and (D) the pp38 mean FI and the ratio of pp38 mean FI to BCR mean FI, both quantified as described for (A), using rabbit anti-pPI3K, -pERK or -pp38, detected with Alexa 488-F(ab′)$_2$ rabbit Ig specific Abs. (B–D) Each data point represents one cell analyzed in one of two independent experiments and the bars indicate the mean ± SD.

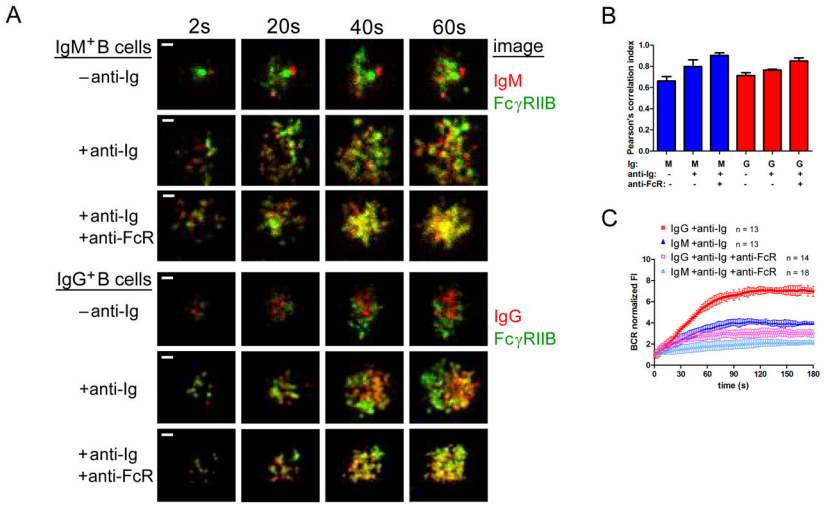

Figure 4. The effect of BCR-FcγRIIB coligation on the response of B cells to anti-Ig-containing fluid lipid bilayers

(A) Representative timelapse TIRF images over a period of 60 s of IgM^+ B cells (top panels) and IgG^+ B cells (lower panels) placed on −anti-Ig or +anti-Ig fluid lipid bilayers or bilayers that contained both anti-Ig and anti-FcγRIIB (anti-FcR). The images shown are of B cells labeled with DyLight 649-Fab anti-IgM (red, top) or -IgG (red, bottom) and Alexa 568-Fab anti-FcγRIIB (green). (Scalebar = 1 μm.) (B) Colocalization of BCR and FcγRIIB after 60 s on −anti-Ig, +anti-Ig or +anti-Ig +anti-FcR bilayers quantified by Pearson's correlation index. The data represent the mean ± SD of: IgM −anti-Ig (n = 4); IgM +anti-Ig (n = 7); IgM +anti-Ig +anti-FcR (n = 7); IgG −anti-Ig (n = 5); IgG +anti-Ig (n = 3) and IgG +anti-Ig +anti-FcR (n = 7) in one of three independent experiments. (C) Normalized BCR FI quantified from several timelapse image series, as in (A), over a period of 180 s from two independent experiments with the bars indicating the mean ± SD.

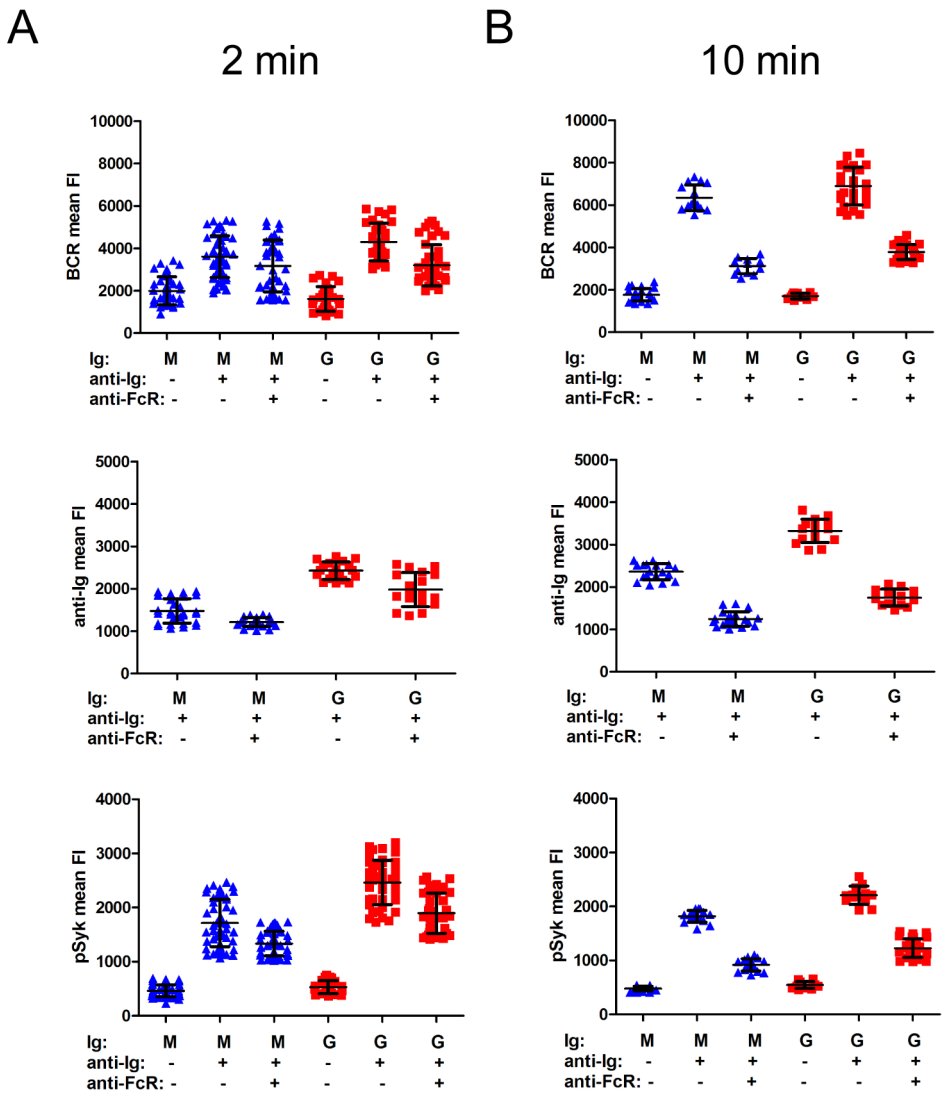

Figure 5. BCR and anti-Ig accumulation at the B cell-anti-Ig-containing bilayer interface are inhibited upon BCR-FcγRIIB coligation

BCR mean FI (top panels), anti-Ig mean FI (middle panels), or pSyk mean FI (bottom panels) (A) 2 min or (B) 10 min after B cells were placed on −anti-Ig, +anti-Ig or +anti-Ig +anti-FcγRIIB (anti-FcR) bilayers quantified from images of fixed B cells labeled with DyLight 649-Fab anti-IgM or -IgG (top panels), of Alexa 568-F(ab′)$_2$ anti-Ig (middle panels), or of Alexa 488-F(ab′)$_2$ Ig specific to anti-pSyk (bottom panels). Each data point represents one cell analyzed in one of two independent experiments for each time point and the bars indicate the mean ± SD.

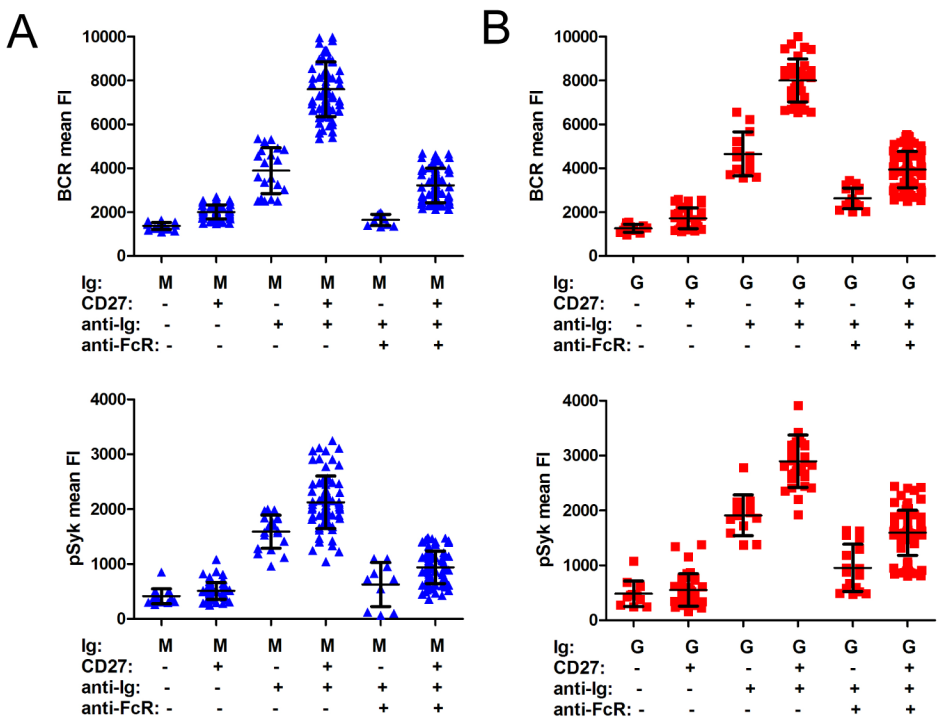

Figure 6. The response of B cell subsets to anti-Ig-containing fluid lipid bilayers

(A) Normalized BCR FI and normalized pSyk FI quantified from TIRF images of IgM^+ B cells or (B) IgG^+ B cells placed on −anti-Ig, +anti-Ig or +anti-Ig +anti-FcγRIIB fluid lipid bilayers for 10 min, fixed and labeled with DyLight 649-Fab anti-IgM or -IgG, Alexa 568-Fab anti-CD27 and Alexa 488-$F(ab')_2$ Ig specific to anti-pSyk. Each data point represents one cell analyzed in one of two independent experiments and the bars indicate the mean ± SD.